Depth Perception Using Blurring and its Application in VLSI Wafer Probing

R.V. Dantu[a], N.J. Dimopoulos[b], R.V. Patel, and A.J. Al-Khalili

Department of Electrical and Computer Engineering, Concordia University, Montreal, Canada, and (a) Bell-Northern Research Ltd., Ottawa, Canada, and (b) Department of Electrical and Computer Engineering, University of Victoria, Victoria, Canada.

Abstract: In this paper, we present a technique for measuring the amount of blur of an edge and using this information to determine the distance of a micromanipulator probe from a wafer surface in very large scale integration (VLSI) wafer probing. In this application, a soft and reliable touch of the probe with a metal pad in the wafer is a sensitive operation. The wafer is focused and several images of the probe while approaching the wafer are analyzed. In our theory, the amount of blur is calculated from the height of the step edge and the slope of the intensity profile at the zero crossing. Hence, our formula is simple and easy to use. We estimate the distance of the probe from the surface of the wafer and obtain a robust measure, i.e., one which is valid even in the presence of significant noise in the images. In order to validate our methods, we have experimented with various VLSI patterns as backgrounds.

Key Words: machine vision, depth perception, blurring, wafer probing

1 Introduction

Computer vision provides important sensory information in many robotic tasks. Measurement of depth of an object in a scene is very useful information for the success of these tasks. This measurement is required for obstacle avoidance and navigation, pose determination, inspection, manipulation, and assembly of objects [1]. The methods for distance measurement can be categorized into two subclasses. The first is monocular, relying on a single viewpoint. The second is nonmonocular requiring two or more images from cameras displaced laterally along a defined baseline. The depth of an object is calculated by measuring the displacement of image features in these images. In our application, automatic wafer probing, we have used the monocular method for obtaining the depth information. The description of this method and the experimental results are described in this paper.

Recent developments in VLSI wafer design indicate a shift towards design for testability [2]. The semiconductor parameters obtained through tests during fabrication improve the monitoring of the ongoing process quality and therefore the yield. The need for such process control and its yield benefits are discussed in [3] and [4]. In wafer testing, metallic probes are used to inject test vectors or to check for continuity [4]. Input and output or test pads are used for such probings. The test pads are intermediate test points provided during layout design to increase testability. These test pads have linear dimensions of the order of 10 microns or less. Also, several probings are required for testing each parameter. The accurate and sensitive operation of touching a probe onto a pad has to be performed repeatedly with good resolution, requiring highly skilled labor. So far, to our knowledge, no work has been reported for automatic testing of the wafers for semiconductor parameters during manufacturing. We are presently developing a micromanipulator system for automating such high resolution tasks as wafer probing [5]. The system is being automated with visual information being used for feedback.

1.1 Experimental Set-up

Our set-up consists of a VLSI wafer probing station complete with a microscope, probe platform, probes, wafer chuck, and a 256 × 256 CCD camera. Through-the-microscope images can be captured,

Address reprint requests to: R.V. Dantu, Bell-Northern Research Ltd., Ottawa, Canada KIY 4H7.

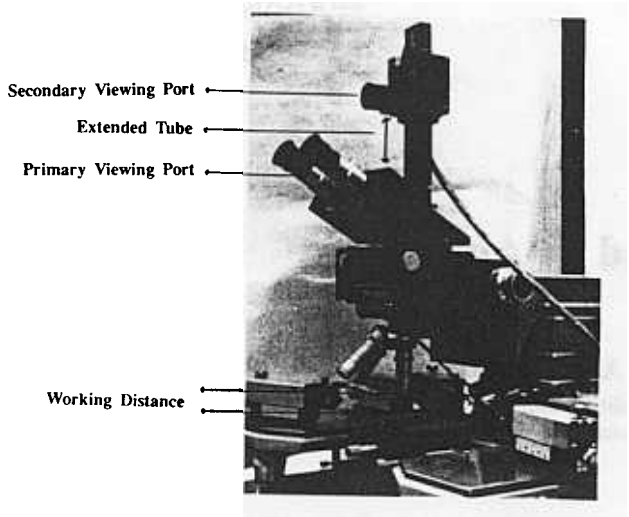

Figure 1. The experimental set-up.

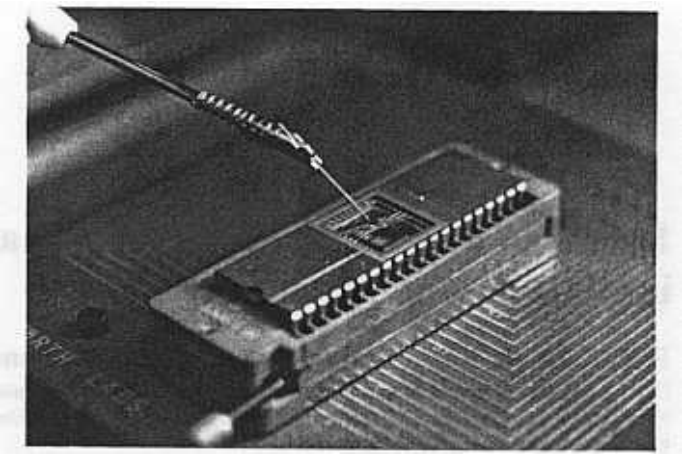

Figure 2. Figure showing the probe approaching the pad in the experimental set-up.

displayed and transferred to back-end processors for further processing. The experimental set-up is shown in Figure 1. In this set-up, the probe tips are fixed obliquely to the optical axis. Also for our experimental work, the wafer is fixed and the probe is lowered using the vertical drive provided by the probe platform of the VLSI test station. The probes are currently under manual control, and can be interfaced to a variety of analyzing equipment for signature or parameter analysis. Currently, our main research effort is in processing the acquired images and extracting parameters related to wafer orientation, pad and probe identification. We are using vision to determine the distance of the probe from the wafer so that accurate guidance of the probe can be achieved.

1.2 Need for Soft Touch of the Probe with the Pad

In order to insert test vectors for signature analysis, the probes have to make good electrical contact with the pads. The probe tip is very fragile and has a thickness of less than a micron. Hence for nondestructive testing of a wafer, the probe should have zero velocity. Our observation has shown that when the probe is being lowered and the velocity of movement is small, upon contact the probe does not initially pierce the pad but slides on the pad without scratching the surface. This phenomenon has given us the means of determining touch nondestructively and also making a good electrical contact. Hence, for a soft touch, guidance of the probe to the pad is a critical operation.

In order to achieve closed loop control of the probe, the position of the probe relative to its target must be established. This includes the proximity of the probe to the wafer which is determined from the depth of the object. Hence, the measurement of the depth of the probe is a vital task in this automation. As described in the experimental set-up, we only have a single view of the probe along the optical axis of the light source. Hence, we have to measure distance using only the available data, that is, the pixel value of the image of the probe. We have used two modes of measurement. The first mode is applied when the probe is far from the wafer. In this case, the pixel values are corrupted by the bright light of the through-the-lens microscope (Figure 2). Hence, we cannot use the absolute values of the probe pixels for measurement. We have devised a method for measuring the distance using the degree of sharpness of the edges in the image. In our application, the scene is comprised of the probe on a background of pads in the VLSI wafer. We have chosen the information around the edges of the probe for the measurement of sharpness. A parameter related to sharpness is the blur around an edge. The amount of blur in a defocused object is inversely proportional to the sharpness of the object. We have developed a method of measuring the blur in the image which we then relate to the distance from the probe to the wafer.

The second mode of measurement is used when the probe is close to, but not touching the wafer. In this mode, the image of the probe is obtained from the difference of two images, one when the probe is completely outside the viewing angle, i.e. an image of background, and the other when the probe is in the vicinity of the wafer. These probe pixels are collected at different instants while the probe approaches the wafer. Suppose the pixel values take a

set of discrete values $\{y_1, y_2, y_3, \ldots, y_n\}$. The mean and variance of the probe (after subtracting the background) is calculated. These parameters start decreasing as the probe gets more and more into focus and begin to increase as the probe starts sliding on the wafer. The dip in variance and mean with respect to distance is identified as touch. Further details are given in [6].

As the probe approaches the wafer, images are captured at various instants and the two methods are applied for every probing operation. In this paper, we discuss the first method for estimating the distance. In the following sections we describe the measurement of the degree of blur of the edges and relate this to the distance of the object. In section 2, the previous work done in perception of depth using a single view is reviewed. A theoretical relation for estimation of blur near the edges is derived in section 3. In section 4, an algorithm for implementation of this relation is described. Finally, the algorithm is applied to a synthetic image and to experimental data, and the results are described in sections 5 and 6, respectively.

2 Past Work in Perception of Depth using Single View

Measurement of depth from focusing/defocusing has been studied by several researchers [7–13]. Initial work concentrated on automatic focusing algorithms. Hausler and Korner [13] used the following focus function for finding the extrema of intensity:

$$R(z) = \sum_{n=0}^{N} \left| \frac{\partial I_n(x, z)}{\partial z} \right| \tag{1}$$

where n is the number of pixels considered and $I(x,z)$ is the intensity function with position x and depth z. They expected $R(z)$ to have only one lowest extremum at the best focus. At this extremum the derivative of the image intensity is zero. This method may be useful for automatic focusing, but in our application since we analyze the grey values of the pixels on one side of the focus plane (i.e., when z is positive or negative), we cannot use this technique. Moreover it is also our intention to estimate the proximity of the probe to the wafer.

A recent approach to depth perception is to measure the degree of blur in the image. To our knowledge, three researchers, Grossmann [14], Pentland [8], and Subbarao [12] have used edge information in measurement of depth of objects. A method of obtaining depth profiles from the sharpness of the edges was first used by Grossmann. The author described this method using experimental data. Initially, the first derivative of the intensity profile perpendicular to the edge direction is computed. The derivative function is bell shaped with a peak at the location of the edge. The width W of this distribution peak is evaluated. Grossmann also suggested a linear relationship between W and the distance d from the focused plane. The constant of proportionality was determined through calibration using experimental data. However, Grossmann concluded that this method is ill defined and sensitive to noise. No further improvements on this method have been reported so far.

Pentland [8] used the second derivative of the intensity profile for calculating the blur in an image. The blurred image of a point object is considered as the point spread function of the optical system. This function is usually modeled by a two-dimensional Gaussian $G(r,\sigma)$ with a spatial constant σ and radial distance r [8]. The value of σ in this model is the radius of the imaged point's "blur circle" or the blur parameter. A direct relation exists between the value of σ and the distance of the imaged point. This is given by the following expression [8].

$$D = \frac{Fv_0}{v_0 - F - \sigma f} \tag{2}$$

where v_0 is the distance between the lens and the image plane (i.e., the sensor location in the camera), f is the f-number of the lens system, F is the focal length of the lens system, and σ is the spatial constant of the point spread function. So, the spread parameter σ of the Gaussian distribution is inversely proportional to the depth D of the object in the scene. It is then possible to determine the distance of an object from the camera by estimating the value of σ.

Pentland [8] used the Laplacian operator of the intensity profiles near the edges for the calculation of σ. He derived the following expression for the calculation of the spread parameter σ of the Gaussian distribution as a linear regression of x^2.

$$ln \frac{\delta}{\sqrt{2\pi\sigma^3}} - \frac{x^2}{2\sigma^2} = ln \left| \frac{C(x,y)}{x} \right| \tag{3}$$

where x is the variable perpendicular to the edge and δ is the step height of the edge. By estimating the value of σ Pentland determined the distance of the image point. In this approach the Laplacian $C(x,y)$ around each edge is calculated. The value of δ is taken to be constant.

Subbarao [12] considered the first derivative of the intensity profiles perpendicular to each edge and

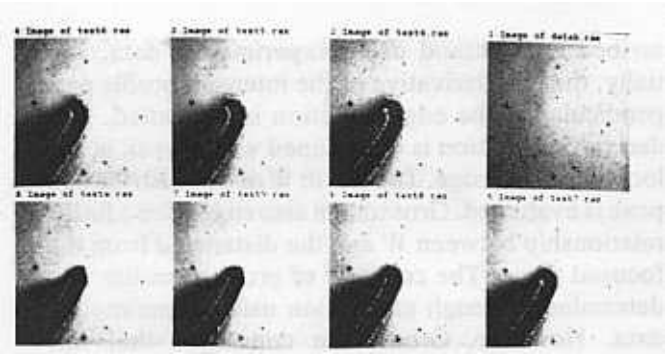

Figure 3. Images of the probe while approaching a uniform background.

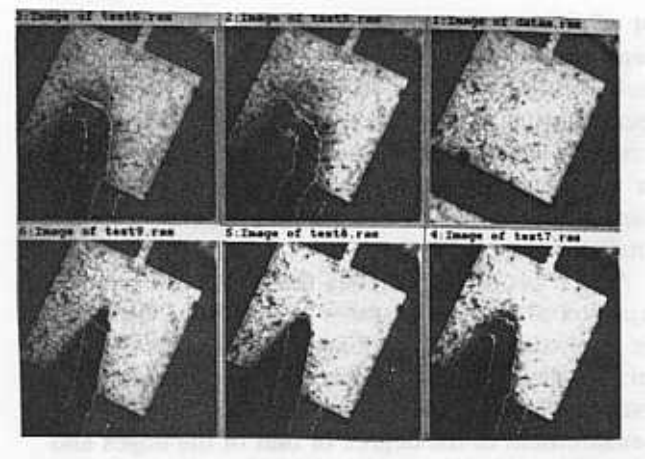

Figure 4. Images of the probe while approaching an I/O pad.

calculated the distance of the object using the formula

$$\sigma = kDs\left[\frac{1}{f} - \frac{1}{u} - \frac{1}{s}\right] \tag{4}$$

where k is the camera constant, f is the focal length of the lens, D is the diameter of the lens, s is the distance from the lens to the image detector plane, u is the distance of the object from the lens and σ is the spread parameter (or blur parameter) of the line spread function. Subbarao computed the first derivative g_x along the intensity gradient by taking the difference of gray values of adjacent pixels (perpendicular to the edge direction). A line spread function $\theta(i)$ is computed using the following equation:

$$\theta(i) = \frac{g_x(i)}{\sum_{i=0}^{N} g_x(i)} \tag{5}$$

where g_x is the first derivative of the intensity function near the edge and N is the number of pixels considered. The spread of σ of the line spread function is computed using the expression for the standard deviation of the line spread function.

$$\sigma = \pm\left[\sum_{i=0}^{N} (i - \bar{i})^2\theta(i)\right]^{\frac{1}{2}} \tag{6}$$

where $\bar{i}$ is the edge location. Although the height of the edge is considered in this approach, the first derivative in a noisy environment results in erroneous depth values.

The two methods described above attempt to estimate the spread σ of the point spread function which is modeled as a Gaussian distribution. They assume that the two surfaces separated by the edge are homogeneous and smooth. We found it difficult to use the above methods in our application as we have a mix of blurred and focused regions. Also the object of interest (i.e., the probe) is at an angle to the optical axis, and therefore the focus varies along its edges. This can be observed in Figures 3 and 4. In addition, in our environment, we do not have smoothed regions or edges for estimation of proximity. The task is made even more difficult by the fact that we have to work with unconstrained illumination, background and hidden surfaces.

In order to eliminate the noise problem, which is particularly accentuated through the use of the Laplacian, we estimate the location of the zero crossing and then use the original data around the zero crossing to estimate σ. In particular, we divide the region around an edge into three sections. The first and third sections belong to the background and the blurred object, respectively, while the second one belongs to the edge itself. We analyze these three parts of the edge separately and calculate the spread σ of the point spread function contributing to the blurring of the edge. By doing so, we arrived at a robust procedure for estimating σ and hence the distance from the tip of the probe to the focal plane, i.e., the target pad. We have applied our algorithm to images of different backgrounds such as those shown in Figures 3 and 4. The following sections describe the theoretical background to our approach, the details of the algorithm, and the results obtained in our application.

3 Theoretical Development

We consider a step edge $f(x)$ with magnitude δ, i.e.

$$f(x) = \begin{cases} k & \text{if } x < 0 \\ k + \delta & \text{if } x \geq 0 \end{cases} \tag{7}$$

The line spread function of the camera with the lens system is modeled as a Gaussian distribution

$$g(x,\sigma) = \frac{1}{\sqrt{2\pi}\sigma} e^{\frac{-x^2}{2\sigma^2}} \tag{8}$$

The step edge is convolved with the line spread function and yields a blurred edge. The blurred edge is represented by the following convolution function $h(x,\sigma)$.

$$h(x,\sigma) = \int_{-\infty}^{\infty} f(\xi)g(x-\xi,\sigma)d\xi \tag{9}$$

$$= k\int_{-\infty}^{0-} g(x-\xi,\sigma)d\xi + \int_{0}^{\infty}(k+\delta)g(x-\xi,\sigma)d\xi \tag{10}$$

$$= k\int_{-\infty}^{\infty} g(x-\xi,\sigma)d\xi + \delta\int_{0}^{\infty} g(x-\xi,\sigma)d\xi \tag{11}$$

Taking the first term on the right hand side

$$k\int_{-\infty}^{\infty} g(x-\xi,\sigma)d\xi = -k\int_{-\infty}^{\infty} g(x-\xi,\sigma)d(x-\xi) = -k\int_{\infty}^{-\infty} g(\tau,\sigma)d\tau \tag{12}$$

where we have changed the variable of integration to $\tau = x - \xi$. Then equation (11) can be written as

$$h(x,\sigma) = k\int_{-\infty}^{\infty} g(\tau,\sigma)d\tau + \delta\int_{-\infty}^{x} g(\tau,\sigma)d\tau \tag{13}$$

Since

$$\int_{-\infty}^{\infty} g(\tau,\sigma)d\tau = 1 \tag{14}$$

and

$$\int_{-\infty}^{0} g(\tau,\sigma)d\tau = \tfrac{1}{2} \tag{15}$$

Equation (13) can be written as

$$h(x,\sigma) = k + \frac{\delta}{2} + \delta\int_{0}^{x} g(\tau,\sigma)d\tau \tag{16}$$

$$h(x,\sigma) = k + \frac{\delta}{2} + \delta\int_{0}^{x} \frac{1}{\sigma\sqrt{2\pi}} e^{\frac{-x^2}{2\sigma^2}} \tag{17}$$

The integral on the right hand side can also be expressed as an error function[1]. However, by differentiating the above equation with respect to x, we get

$$\left|\frac{\partial h(x,\sigma)}{\partial x}\right|_{x=0} = \frac{\delta}{\sigma\sqrt{2\pi}} \tag{18}$$

The function $h(x,\sigma)$ can be represented using piecewise linear segments.

$$h(x,\sigma) = \begin{cases} k & \text{for } x \in (-\infty \ldots p_1) \\ J_1(x,\sigma) & \text{for } x \in (p_1 \ldots p_2) \\ J_2(x,\sigma) & \text{for } x \in (p_2 \ldots) \\ \ldots ? & \ldots ? \\ a_0(\sigma) + a_1(\sigma)x & \text{for } x \in (p_{z-1} \ldots p_{z+1}) \\ J_{z+1}(x,\sigma) & \text{for } x \in (p_{z+1} \ldots p_{z+2}) \\ \ldots ? & \ldots ? \\ k + \delta & \text{for } x \in (p_3 \ldots p_\infty) \end{cases} \tag{19}$$

where $J_1(x,\sigma)$, $J_2(x,\sigma)$ and $J_{z+1}(x,\sigma)$ are piecewise linear functions. Here p_z is the point of zero crossing. In order to calculate σ [using equation (18)], we must calculate the derivative of the blurred edge at its zero crossing and also the height of the step edge δ. This is shown in Figures 5 and 6. In our case, we approximate the blurred edge by a least-squares fit of the piecewise linear segments. Then, we differentiate this function with respect to x and evaluate the result at $x = 0$, i.e., at the point p_z in Figure 5.

$$\left|\frac{\partial h(x,\sigma)}{\partial x}\right|_{x=0} = a_1(\sigma) \tag{20}$$

From equation (18), we obtain an expression for σ as

$$\sigma = \frac{\delta}{a_1(\sigma)\sqrt{2\pi}} \tag{21}$$

We can also estimate δ from Eq. (19) as

$$\delta = h(+\infty) - h(-\infty) \tag{22}$$

where

[1] An error function is defined as $\frac{1}{\sqrt{2\pi}}\int_0^x e^{\frac{-t^2}{2}} dt$

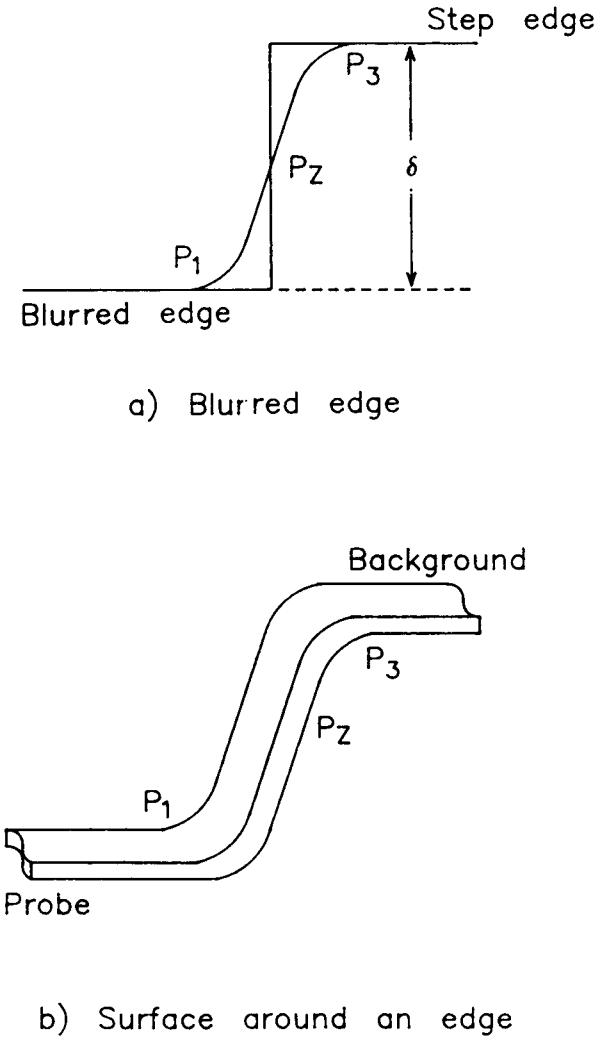

Figure 5. Ideal edge profile.

$$h(\pm\infty) = \lim_{x \to \pm\infty} h(x,\sigma) \tag{23}$$

The standard deviation σ (which from now onward we shall call "the blur parameter") of the Gaussian distribution allows us to determine the distance of the object using equation (2) or (4). We have used the following algorithm to obtain different parameters in equation (21).

4 Algorithm

In this section we describe the different steps in evaluating equation (21). These processing steps include the following: (a) obtaining an edge map of the probe, (b) using this estimate to find the actual zero crossing and hence the "blur parameter" σ along each edge, and (c) correlating σ with the measured distance of the probe from the surface of the pad.

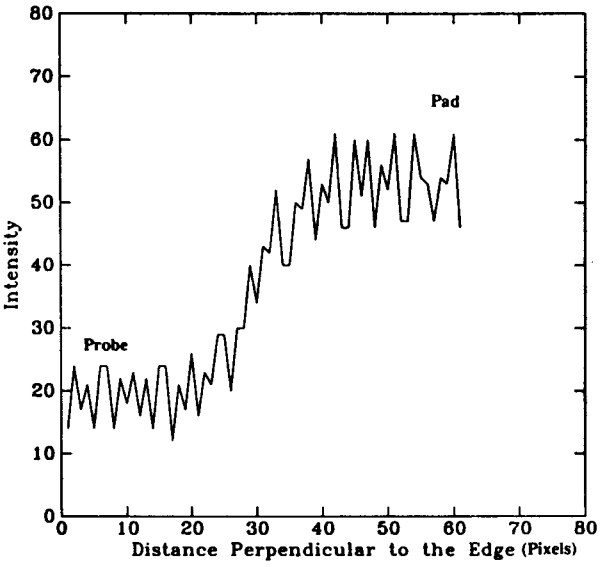

Figure 6. Edge profile for Figures 3 and 4.

4.1 Generation of an Edge Map of the Probe

For analyzing the neighborhood of a blurred edge we need to determine the location of the edge. The procedure for obtaining the edge map of the probe is described here. The image of the VLSI wafer consists of pads, probes, and layout patterns. Due to bright through-the-lens illumination and different reflection characteristics of the materials of the wafer (e.g., substrate, metal, and poly-silicon) the image is corrupted by a considerable amount of noise. Hence, for the extraction of edges, we smooth the image using a neighborhood of 3 × 3 pixels. The probe, pad, and background have distinct grey levels; we use these levels as threshold values for creating their images. The edge map of the probe is generated from the zero crossings of the Laplacian of the probe image. Such an edge map is shown in Figures 3 and 4.

4.2 Interpolation of the Edge Map

Due to the presence of noise, the edge map obtained in the previous section is not continuous, but contains gaps within the neighboring edges. These gaps are "filled in" with linear segments as follows: If (x_1,y_1) and (x_2,y_2) are the end points of two adjacent regions, then the new point (x_{new},y_{new}) at a distance d from (x_1,y_1) is calculated using the following equation.

$$x_{new} = Int\left[x_1 \pm \left(\frac{d_i^2}{1+m^2}\right)^{\frac{1}{2}}\right] \tag{24}$$

$$y_{new} = Int\left[y_1 \pm \left(\frac{d_i^2}{1 + \frac{1}{m^2}}\right)^{\frac{1}{2}}\right] \tag{25}$$

where m is the slope of the line joining (x_1,y_1), (x_2, y_2). The operator *Int* produces a rounded value of the right hand side of the above formula.

4.3 Chaining of Edges

The probe is a conical object and the projection of this on the image plane has a triangular shape. We can observe this in Figures 3 and 4. The edges in the image plane represent the boundaries of the conical surface of the probe. Also, the probe is at an angle to the optical axis of the microscope. The end point of the tip is considered as the first element of the edge map. The next element of the edge map is located by searching the neighborhood and then linking to the first one. This chaining is continued up to the mount of the probe, i.e., until the farthest end is reached. This procedure results in a linked list of the edges starting from the tip to the mount.

4.4 Determination of Pixels Perpendicular to Edges

The blurring around each edge in the edge map is analyzed. More specifically, we have to analyze the pixels perpendicular to each edge. This section describes the procedure for determining these pixels.

Each probe pixel in the image plane is the vertical projection of the three-dimensional surface of the probe. Also, the grey levels of the pixels depend on the blurring due to defocusing. So the grey level profile around all the edges is considered for the calculation of the blur parameter σ. As per our assumption in equation (7), a profile of the edge is perpendicular to the edge. This profile is a set of image pixels lying normal to the edge under consideration. For each edge at (x,y) with slope m, we calculate a point (x_i,y_i) in the direction perpendicular to the edge and at a distance d_i from (x,y) using the following formula:

$$y_i = Int\left[c \pm \left(\frac{d_i^2 + x^2 + (y-c)^2}{\left[1 + \frac{1}{m}\right]^2}\right)^{\frac{1}{2}}\right]$$

$$x_i = Int\left[\frac{y-c}{m}\right] \tag{26}$$

By varying the distance $d_i (i = 1, 2, 3, \ldots)$ we find all the points (x_i,y_i) in the perpendicular direction. The operator *Int* in the above-mentioned formulas produces the rounded value of the right hand side. Sixty pixels ($i = 1, 2, 3, \ldots 60$) in the perpendicular direction are considered for each edge. This number is determined experimentally to give a sufficiently detailed profile for most of the edges in our images. The edges and the region of pixels in the perpendicular direction are highlighted in Figures 3 and 4.

4.5 Extraction of the Three Regions in an Edge Profile

In this section we describe the procedure for determining the three regions in the edge profile. The vertical cross section (profile of the edges) obtained with the above procedure (previous section) constitutes the blurred edge. The degree of the blur σ at each edge point can be calculated from the slope of the edge at its zero crossing, and the height of the edge [see Eq. (21)]. In our application, the height of the edge is the grey level difference between the two regions, i.e., the body of the probe and the background. The edge location computed using a Laplacian (described in section 4.1) may not be the true zero crossing of the edge profile. Hence we recalculate the zero crossing of the Laplacian using the following procedure. All the grey levels along the perpendicular direction are fitted with a polynomial. A zero crossing of the second order derivative of this polynomial is taken as the true edge. The shape of the edge profile is shown in Figure 5. The point p_z denotes the zero crossing and points p_1 and p_3 denote the two extrema of the edge. The points p_1 and p_3 for every edge profile are obtained by detecting the zero crossings of the third order derivative of the edge profile. All the grey values of the points with coordinates in the range from the first point on the perpendicular direction to p_1 are considered to belong to the body of the probe. The grey levels of points with coordinates in the range (p_1, p_3) are considered to belong to the edge. Finally, the grey levels of points with coordinates from p_3 to the last point on the perpendicular direction (point 60 in our case) are considered to belong to the background. These three sets of grey levels are used in the next step to calculate the blur parameter σ.

4.6 Piecewise Plane Fitting Around the Surface of the Edge

To determine the accurate slope of the edge profile (even for noisy profiles) we have used the neighboring edge profiles. This operation is valid since all the edge profiles are formed by a single object (probe) and the background. Thus, in order to evalu-

$$y_{new} = Int\left[y_1 \pm \left(\frac{d_i^2}{1 + \frac{1}{m^2}}\right)^{\frac{1}{2}}\right] \tag{25}$$

where m is the slope of the line joining (x_1,y_1), (x_2, y_2). The operator *Int* produces a rounded value of the right hand side of the above formula.

4.3 Chaining of Edges

The probe is a conical object and the projection of this on the image plane has a triangular shape. We can observe this in Figures 3 and 4. The edges in the image plane represent the boundaries of the conical surface of the probe. Also, the probe is at an angle to the optical axis of the microscope. The end point of the tip is considered as the first element of the edge map. The next element of the edge map is located by searching the neighborhood and then linking to the first one. This chaining is continued up to the mount of the probe, i.e., until the farthest end is reached. This procedure results in a linked list of the edges starting from the tip to the mount.

4.4 Determination of Pixels Perpendicular to Edges

The blurring around each edge in the edge map is analyzed. More specifically, we have to analyze the pixels perpendicular to each edge. This section describes the procedure for determining these pixels.

Each probe pixel in the image plane is the vertical projection of the three-dimensional surface of the probe. Also, the grey levels of the pixels depend on the blurring due to defocusing. So the grey level profile around all the edges is considered for the calculation of the blur parameter σ. As per our assumption in equation (7), a profile of the edge is perpendicular to the edge. This profile is a set of image pixels lying normal to the edge under consideration. For each edge at (x,y) with slope m, we calculate a point (x_i,y_i) in the direction perpendicular to the edge and at a distance d_i from (x,y) using the following formula:

$$y_i = Int\left[c \pm \left(\frac{d_i^2 + x^2 + (y-c)^2}{\left[1 + \frac{1}{m}\right]^2}\right)^{\frac{1}{2}}\right]$$

$$x_i = Int\left[\frac{y-c}{m}\right] \tag{26}$$

By varying the distance $d_i (i = 1, 2, 3, \ldots)$ we find all the points (x_i,y_i) in the perpendicular direction. The operator *Int* in the above-mentioned formulas produces the rounded value of the right hand side. Sixty pixels ($i = 1, 2, 3, \ldots 60$) in the perpendicular direction are considered for each edge. This number is determined experimentally to give a sufficiently detailed profile for most of the edges in our images. The edges and the region of pixels in the perpendicular direction are highlighted in Figures 3 and 4.

4.5 Extraction of the Three Regions in an Edge Profile

In this section we describe the procedure for determining the three regions in the edge profile. The vertical cross section (profile of the edges) obtained with the above procedure (previous section) constitutes the blurred edge. The degree of the blur σ at each edge point can be calculated from the slope of the edge at its zero crossing, and the height of the edge [see Eq. (21)]. In our application, the height of the edge is the grey level difference between the two regions, i.e., the body of the probe and the background. The edge location computed using a Laplacian (described in section 4.1) may not be the true zero crossing of the edge profile. Hence we recalculate the zero crossing of the Laplacian using the following procedure. All the grey levels along the perpendicular direction are fitted with a polynomial. A zero crossing of the second order derivative of this polynomial is taken as the true edge. The shape of the edge profile is shown in Figure 5. The point p_z denotes the zero crossing and points p_1 and p_3 denote the two extrema of the edge. The points p_1 and p_3 for every edge profile are obtained by detecting the zero crossings of the third order derivative of the edge profile. All the grey values of the points with coordinates in the range from the first point on the perpendicular direction to p_1 are considered to belong to the body of the probe. The grey levels of points with coordinates in the range (p_1, p_3) are considered to belong to the edge. Finally, the grey levels of points with coordinates from p_3 to the last point on the perpendicular direction (point 60 in our case) are considered to belong to the background. These three sets of grey levels are used in the next step to calculate the blur parameter σ.

4.6 Piecewise Plane Fitting Around the Surface of the Edge

To determine the accurate slope of the edge profile (even for noisy profiles) we have used the neighboring edge profiles. This operation is valid since all the edge profiles are formed by a single object (probe) and the background. Thus, in order to evalu-

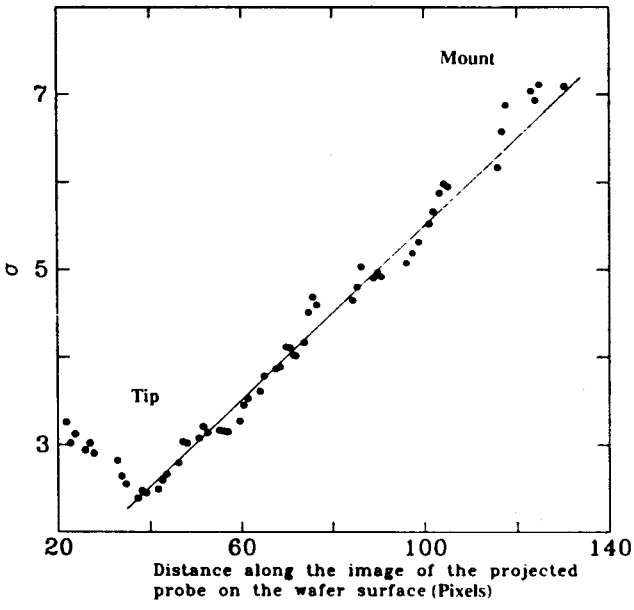

Figure 8. Fitting a straight line for σ along the probe.

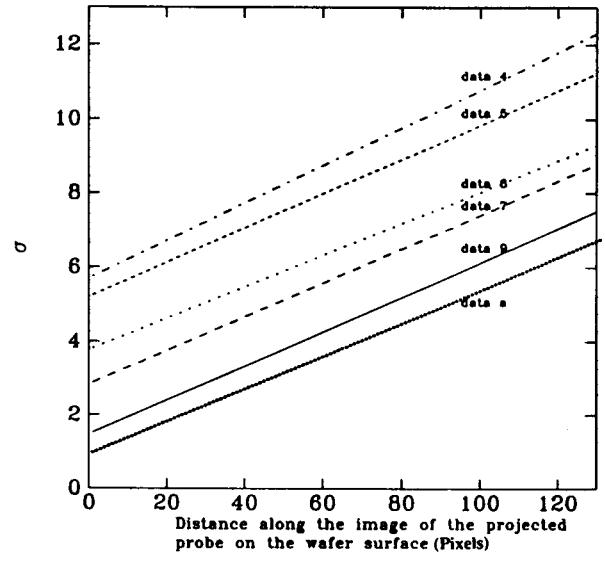

Figure 9. Variation of σ along the probe for Figure 3.

the calculated value of σ for ten sets of experimental data is discussed in section 6.2. Finally, with this value of σ, the actual distance can also be evaluated using equation (2) or (4). For this, we require the optical constants obtained from the specifications of the microscope and the camera [8, 12].

6.1 Diffusion Layer as Background

Images of uniform background, i.e., images of non-inscribed wafers are considered in this section and the value of σ is calculated using equation (21). A sequence of frames (images of the probe and background) with known distance is captured. These are shown in Figure 3. We can observe in the figure that the image of the probe is blurred when the probe is "far" from the wafer. The last frame in Figure 3 represents the probe when it is touching the wafer. In our experimental set-up the probe is at an angle to the optical axis. Since the microscope is focused on the wafer, the mount of the probe is more blurred compared to the tip. Although the wafer surface in Figure 3 appears smooth, the grey level surface is rough due to the specular and diffused noise (Figure 6). The situation is further aggravated by the blurred image of the probe. Even then, the results are satisfactory.

The edge profile of the probe is obtained as described in section 4. Consecutive images are analyzed while the probe is approaching the wafer. For each image, the value of σ at every edge of the probe is calculated. The variation of σ along the surface of the probe (while it is touching the surface) is shown in Figure 8. Each point in this figure represents the value of σ for the corresponding edge in the image of the probe. Least-squares fitting of a straight line through all these points is also shown in Figure 8. We can observe from this figure that the probe orientation with respect to the optical axis can be estimated from the measurement of σ. This is a useful feature in understanding orientation using blurring.

The procedure described above, i.e., fitting a straight line along the probe, is repeated for all the images while the probe is approaching the wafer. The variation of σ for each image (represented by a straight line) of the probe is shown in Figure 9. In this figure, all the lines are staggered and almost parallel to each other. The bottom line represents the image of the probe while touching the wafer. The top line represents the image of the probe farthest away from the wafer surface. This confirms our assumption that the probe is approaching the wafer through movement along the z axis.

6.2 Metal Pad as Background

The second set of images considered as the input/output (I/O) pads. A sequence of images was analyzed as the probe approaches the wafer. These are shown in Figure 4. There are two visible layers in the image of the wafer; metal and substrate. The metal region is bright and consequently has very high contrast with the probe. The tip is positioned at the center of the I/O pad. As the tip of the probe is very sharp, the loci of the perpendiculars to the edges consist of different regions in the image. Also, the edge profiles at the point of contact are corrupted by the high intensity reflections from the metal sur-

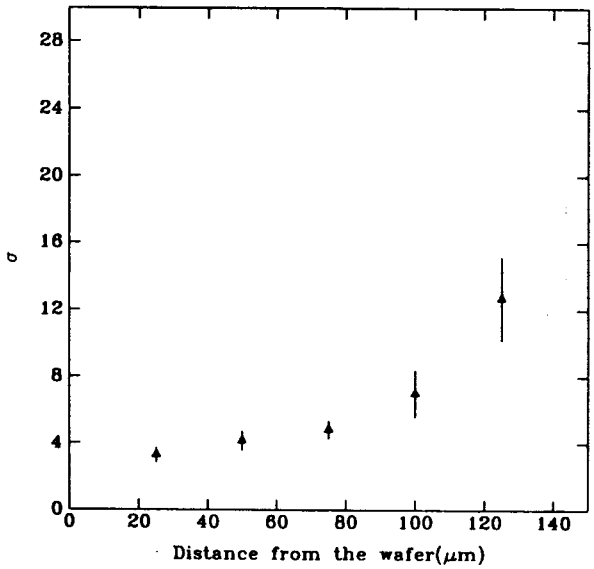

Figure 10. Deviation from mean value of σ.

face. Moreover, the surface of the probe near the boundary of the metal pads does not have a homogeneous background (Figure 4). This is not desirable because irregular edge profiles result in inaccurate σ values. Because of the above-mentioned reasons, we have considered the edge profiles over a small region (30 edge profiles) near the tip and calculated the average value of σ for this region. The values of σ for various frames while the probe is approaching the wafer are shown in Figure 10.

The final objective for the measurement of σ is the controlled guidance of the probe to the target pad. The degree of confidence in the measurement of σ and subsequently the estimation of distance is an important consideration in any new technique, and ours is no exception. We describe below some experimental results to meet this consideration. One useful observation in our application is that only metal pads are used as contact points in any VLSI design. Therefore, we have considered 10 sets of images, where each set contains images of the probe while approaching different metal pads. For each image of the probe, the value of σ is calculated as described in the previous paragraph. The mean values of all 10 sets are plotted against the distance and are shown in Figure 10. The deviation of σ for each distance is also shown. By observing the figure, we can conclude that for any calculated value of σ it is possible to estimate the distance of the probe and hence the required Z-drive to the probe.

7 Conclusions

The semiconductor industry is one of the principal beneficiaries of computer vision research. It is also a major buyer of vision hardware and software. The high precision required by this industry can only be achieved using high resolution optics and vision systems, particularly since the introduction of VLSI. The increased complexity and small feature size of VLSI circuits have created challenging research problems in several manufacturing areas. Machine vision has been successfully applied to wafer inspection, die and wire bonding, and testing. However, there are several areas such as automatic wafer probing where further research of a more interdisciplinary nature is required. In wafer probing, metallic probes are used to contact the surfaces of the wafer. Compliant and reliable probing is a highly skilled operation which has to be repeated with good accuracy. In this paper, we described a method for estimating the depth of an object, which is used in guiding the probe to the pad. This method estimates the depth of an object using information concerning blurring around the edges.

The methods suggested by Pentland [8, 9] and Subbarao [12] use second and first derivatives of the intensity profiles perpendicular to the edge. Because of the derivative calculations along the entire cross section, these methods are sensitive to noise and are not suitable for some uncontrolled environments, like the application considered in this thesis, where the image is corrupted by noise due to incorrect illumination, motion, etc. In our method, we need to find the slope of the edge profile at one point, i.e., at the zero crossing. In order to estimate the slope of an edge, even in the presence of noise, we fit a plane surface in the neighborhood of the zero crossing. The slope of this plane is used in calculating σ. In contrast to other methods, our estimates the slope directly from the image, which is hence less susceptible to noise.

In order to confirm our theory as well as to test it in a real environment, we have applied it to determine the distance of a probe from the surface of a VLSI wafer. We have considered 10 sets of images of different VLSI wafers belonging to different batches in the fabrication process. The parameter which is uniformly varied in all these images is the blur parameter σ. It can be observed from Figures 8 and 9 that similar values of σ were obtained for different backgrounds. This confirms our theory and shows that σ can be used as a measure in guiding the probe to its destination on the wafer. The deviation in the measurement of σ can be reduced by considering a higher number of grey levels (e.g. 256) than in the present set-up (64 levels). Another concern is in the measurement of δ [the height of the step edge in equation (21)]. The values of δ need to be calibrated for different settings of the lamp illumination. This will further improve the measure-

ment. Due to the above-mentioned limitations, we use this method for coarse measurement of distance of the probe from the wafer.

Another interesting observation is that a smoother variation of σ is observed for a uniform background, e.g. a single layer of the background material (Figure 3), than for nonuniform backgrounds, e.g. one having several layers (Figure 4). Hence a blurred object on a uniform background gives a more accurate measure of the distance from the object to the background. Also, we observe that the slope of the plane near zero crossings, for different backgrounds, varies very significantly and agrees with common experience that a blurred object looks sharper against a high contrast background than against a low contrast one. This type of information may also be used for identifying boundaries between different regions. Our human visual system can neither estimate nor identify the vertical orientation of the probe by viewing along the optical axis (see Figures 3 and 4). But it is possible through machine vision to obtain this information by measuring the blur parameter of the blurred object (Figure 9). This interesting result may be useful in other applications of machine perception.

References

Beddoe-Stephens C (1982) Semiconductor wafer probing, Test and Measurement World, pp. 33–35

Dantu R, (1990) A Computer Vision System for VLSI Wafer Probing. Ph.D. thesis, Department of Electrical and Computer Engineering, Concordia University, Montreal, Quebec, Canada

Dantu RV, Dimopoulos NJ, Patel RV, Al-Khalili AJ (1989) Micromanipulator vision for wafer probing, IEEE Transactions on Semiconductor Manufacturing, vol. 2, pp. 114–117

Engl WL (1986) Process and Device Modelling. Amsterdam: North-Holland Publishing Company

Grossmann P (1987) Depth from focus, Pattern Recognition Letters, vol. 5, pp. 63–69

Hausler G, Korner E (1984) Simple focusing criterion, Applied Optics, vol. 23

Hwang T, Clark JJ, Yuille AL (1989) A depth recovery algorithm using defocus information, IEEE Computer Society International Conference on Pattern Recognition, San Diego, California

Marapane SB, Trivedi MM (1989) Region-based stereo analysis for robotic applications, IEEE Transactions on Systems, Man, and Cybernetics, vol. 19, pp. 1447–1464

Pentland AP (1987) A new sense for depth of field, IEEE Transactions on Pattern Analysis and Machine Intelligence, vol. 9, pp. 523–531

Pentland AP, Darrel T, Turk M, Huang W (1989) A simple real-time range camera, in IEEE Computer Society International Conference on Computer Vision and Pattern Recognition, San Diego, California

Subbarao M, Natarajan G (1988) Depth recovery from blurred edges, IEEE Computer Society International Conference on Computer Vision and Pattern Recognition, Ann Arbor, Michigan, pp. 498–503

Subbarao M (1989) Machine Vision for Inspection and Measurement, New York, Academic Press, pp. 101–126

Subbarao M (1988) Parallel depth recovery by changing camera parameters, IEEE Computer Society International Conference on Computer Vision, Florida, pp. 149–155

Williams TW (1986) VLSI Testing. Amsterdam: North-Holland Publishing Company